Pergamon

PII: S0022-4073(98)00020-X

J. Quant. Spectrosc. Radiat. Transfer Vol. 60, No. 3, pp. 463–474, 1998

Printed in Great Britain
0022–4073/98 $19.00 + 0.00

EXPERIMENTAL SIZE DETERMINATION OF SPHEROIDAL PARTICLES VIA THE *T*-MATRIX METHOD

ARTURO QUIRANTES† and ANGEL DELGADO

Departamento de Física Aplicada, Facultad de Ciencias, Universidad de Granada, 18071 Granada, Spain

Abstract—Light scattering (LS) properties have been used for determining the size and shape in colloidal suspensions of hematite particles in water. The system has been approximated by a suspension of randomly oriented, monodisperse, spheroidal particles with an equivalent-volume-diameter d_{eq} and an axial ratio, or eccentricity, $\varepsilon = a/b$ (b = revolution axis), in the single-scattering mode. Relative intensity measurements have been taken at several angles, and the results have been compared with theoretical models obtained by combining Waterman's Extended Boundary Condition Method (EBCM) together with Mishchenko's analytical averaging scheme for randomly oriented particles. Both full and depolarized LS have been measured and fitted to theoretical curves. While both methods give good agreement on particle size, shape is not always characterized unequivocally with full LS. The problem is overcome by using depolarized LS, which, for spherical particles, is zero; fit between experimental depolarized LS and theoretical predictions give the correct value of eccentricity, as well as a more accurate value of d_{eq}. This is an experimental validation that depolarized LS can be useful for determining size and shape of real particle systems.

1. INTRODUCTION

The field of colloidal physics has long been closely associated to light scattering (LS) ever since Gustav Mie's paper[1] on light scattering by spheres (which was, essentially, written as a colloidal physics paper). The so-called Mie theory could be used not only to explain LS phenomena in colloidal systems, but it can also be used to extract information on particle size by solving the inverse problem, namely: by analyzing the scattered field, describe the particle/s responsible for the scattering.[2,3] This can be achieved by trial and error, calculating a given LS property for many different particle sizes, until a size is found whose scattering feature most closely resembles experimental data. Particle sizing based in Mie theory is found extensively in the literature;[4-7] its extension to particle size distributions is straightforward.[8–14] However, as Mie's paper is so much cited even today (88 times in 1.996 alone), it is worth to remember its last words: "In order to complete the theory, it is absolutely necessary to investigate also the behavior of ellipsoidal particles." Certainly, Mie theory is not applicable in the case of nonspherical particles, and other theories had to be developed if LS is still to play a role in particle sizing.

In the present paper, LS properties of spheroidal particles have been observed in the laboratory and compared to theoretical results obtained by means of the extended boundary condition method (EBCM), also known as *T*-matrix. This method is suitable for any kind of particle geometry (although it is most efficient for axially symmetric particles), and its nature allows for an analytical orientation averaging in an efficient way, therefore reflecting a statistical-approach philosophy suggested by Bohren and Singham.[15] Full and depolarized LS have been compared and their capabilities assessed for their eventual use as size/shape characterization methods. Conclusions have been confirmed by computations for several size and shape parameters. Since a single refractive index and a limited set of size parameters have been used in the computations, results must be taken

† Author to whom correspondence should be addressed. e-mail: aquiran@goliat.ugr.es.

with some precaution, although the agreement with data from the literature suggests general features for all kinds of particles within a certain size range.

2. THEORY

Waterman's T-matrix approach[16–18] relies, in the first place, in an expansion of both incident and scattered time-independent electrics fields $\boldsymbol{E}_{\mathrm{inc}}(\boldsymbol{r})$, $\boldsymbol{E}_{\mathrm{sca}}(\boldsymbol{r})$ in vector spherical harmonics $\boldsymbol{M}_{\mathrm{mn}}(k\boldsymbol{r})$, $\boldsymbol{N}_{\mathrm{mn}}(k\boldsymbol{r})$ outside a circunscribing sphere of the scattering particle:[19–21]

$$\boldsymbol{E}_{\mathrm{inc}}(\boldsymbol{r}) = \sum_{n=1}^{\infty} \sum_{m=-n}^{n} [a_{mn} Rg\boldsymbol{M}_{mn}(k\boldsymbol{r}) + b_{mn} Rg\boldsymbol{N}_{mn}(k\boldsymbol{r})], \tag{1}$$

$$\boldsymbol{E}_{\mathrm{sca}}(\boldsymbol{r}) = \sum_{n=1}^{\infty} \sum_{m=-n}^{n} [p_{mn}\boldsymbol{M}_{mn}(k\boldsymbol{r}) + q_{mn}\boldsymbol{N}_{mn}(k\boldsymbol{r})]. \tag{2}$$

Due to the linearity of Maxwell's equations and boundary conditions, the scattered field coefficients (p_{mn}, q_{mn}) are related to the incident field coefficients (a_{mn}, b_{mn}) by means of a transition (T) matrix as follows:[16,20]

$$p_{mn} = \sum_{n'=1}^{\infty} \sum_{m'=-n'}^{n'} [T^{11}_{mnm'n'} a_{m'n'} + T^{12}_{mnm'n'} b_{m'n'}], \tag{3}$$

$$q_{mn} = \sum_{n'=1}^{\infty} \sum_{m'=-n'}^{n'} [T^{21}_{mnm'n'} a_{m'n'} + T^{22}_{mnm'n'} b_{m'n'}]. \tag{4}$$

Since the T matrix elements depend on the particle (size, shape, composition and orientation), but not on the nature of the incident and scattered fields, they must be calculated only once and then used for any directions of light incidence and scattering by using rotation transformations.[22,23]

The elements of this so-called natural T matrix can then be linked to the Mueller matrix $\boldsymbol{F}(\theta)$ for particles in random orientation. This can be achieved in two steps. First, the Mueller matrix elements are expanded in a set of generalized spherical functions[24–26] $\boldsymbol{P}^{\mathrm{s}}_{mn}(\cos\theta)$:

$$F_{11}(\theta) = \sum_{s=0}^{\infty} a_1^s P_{00}^s(\cos\theta), \tag{5}$$

$$F_{22}(\theta) + F_{33}(\theta) = \sum_{s=2}^{\infty} (a_2^s + a_3^s) P_{22}^s(\cos\theta), \tag{6}$$

$$F_{22}(\theta) + F_{33}(\theta) = \sum_{s=2}^{\infty} (a_2^s - a_3^s) P_{2-2}^s(\cos\theta), \tag{7}$$

$$F_{44}(\theta) = \sum_{s=0}^{\infty} a_4^s P_{00}^s(\cos\theta), \tag{8}$$

$$F_{12}(\theta) = \sum_{s=2}^{\infty} b_1^s P_{02}^s(\cos\theta), \tag{9}$$

$$F_{34}(\theta) = \sum_{s=0}^{\infty} b_2^s P_{02}^s(\cos\theta), \tag{10}$$

(for randomly oriented, axially symmetric particles, all other Mueller elements are zero[3] except for $F_{21} = F_{12}$ and $F_{43} = -F_{34}$). Second, the expansion coefficients a_i^s, b_i^s are related to the natural T-matrix elements; the whole procedure was developed in a key paper by Mishchenko[27] and will not be repeated here; it will only be remarked that his use of orthogonality and sum relations for Clebsch–Gordan coefficients and Wigner's D functions greatly speeds computations and overcomes the problem of numerically integrating on three different angles. Finally, the Mueller matrix links the incident $\boldsymbol{I}_i$ and scattered $\boldsymbol{I}_s$ light beams:

$$I_{\mathrm{s}} = \frac{C_{\mathrm{sca}}}{4\pi R^2} \boldsymbol{F}(\theta) I_i \tag{11}$$

where R is the particle-detector distance, C_{sca} is the scattering cross section, and $\boldsymbol{I} = (I, Q, U, V)$ is the Stokes vector of a light beam. The following convention is adopted:[3] I is the total irradiation, Q is the difference between the intensities of light polarized parallel and perpendicular (respective to a reference plane), U is the difference between light polarized in the directions $\gamma + 45^\circ$ and $\gamma - 45^\circ$ (γ being the clockwise angle above the scattering plane), and V is the difference between right-handed and left-handed circularly polarized light.

3. EXPERIMENTAL DETAILS

In our experimental setup, incident light from a monochromatic source (75 mW 2213 Cyonics Argon Ion laser, $\lambda_0 = 488$ nm, polarized perpendicularly to the scattering plane) incides on the colloidal suspension; the light scattered at a given angle θ is collected by a Malvern 4700 PCS (Photon Correlation Spectroscopy) spectrometer, working in light-gathering mode. This scheme (the use of only a light source, a sample and a light counter) has been used in many size determinations of natural systems.[28–30] While natural (unpolarized) incident light is a common feature in many systems, some applications such as lidar scattering on raindrops or atmospheric aerosols, require, or start from, polarized incident radiation.[25,31–32] Polarized incident light is also routinely used in particle sizing in fields such as colloidal physics and pharmaceuticals; the reader is referred to Ref. 2 for an extensive review.

When no analyzing element (such as polarizers or quarter-wave plates) are located between the suspension and the photomultiplier tube, the scattered light will then be described by Eq. (11):

$$I_{sca} = \frac{C_{sca}}{4\pi R^2} \begin{pmatrix} F_{11} & F_{12} & 0 & 0 \\ F_{12} & F_{22} & 0 & 0 \\ 0 & 0 & F_{33} & F_{34} \\ 0 & 0 & -F_{34} & F_{44} \end{pmatrix} \begin{pmatrix} I_i \\ -I_i \\ 0 \\ 0 \end{pmatrix} = C \begin{pmatrix} F_{11} - F_{12} \\ F_{12} - F_{22} \\ 0 \\ 0 \end{pmatrix} \tag{12}$$

so that the collected scattered light (henceforth "full LS") is proportional to the difference $F_{11}(\theta) - F_{12}(\theta)$. The proportionality constant C depends on experimental details such as the particle–detector distance or the quantum efficiency of the photomultiplier; in order to eliminate these new parameters, both theoretical and experimental intensities have been normalized to a reference angle θ_0, $i(\theta) = I(\theta)/I(\theta_0)$. A second set of measurements were carried out by placing a cross polarizer between sample and PMT in such a way that the transmission axis of the polarizer

Fig. 1. Transmission electron micrograph of hematite samples A (a) and B (b).

Table 1. Size and shape of samples A and B as obtained from Electron Microscopy (EM) data

Sample	d_{eq} (nm)	ε
A	160 ± 30	0.30 ± 0.08
B	210 ± 20	0.40 ± 0.04

is perpendicular to the polarization direction of the incident beam. The scattered signal (henceforth "depolarized LS") is now proportional to the difference $F_{11}(\theta) - F_{22}(\theta)$; the normalization procedure remains the same as above.

Colloidal solutions of elongated hematite particles in water were synthesized by precipitacion from homogeneous solutions.[33–36] Two suspensions, labelled A and B, were obtained by varying the initial conditions (Fe^{3+} ion concentration, pH, temperature, aging time, etc). Ultrasonication has been used to reduce to a minimum the chance of aggregation. Transmission Electron microscopy (HRTEM Zeiss EM-130) photographs (Fig. 1) show that both samples are composed of spheroidal, nearly monodisperse particles with axes a and b (b = revolution axis). Short-to-long axis ratio distributions show that eccentricity values are very similar to all particles, thus indicating that 3-D projections on 2-D photographs do not have much relevance. Particles will thus be described by the equivalent-volume diameter $d_{eq} = (a^2 b)^{1/3}$ and the eccentricity $\varepsilon = a/b$ (Table 1). Observation of the absence of Tyndall effect and linearity of absolute intensity on concentration and incident light power ensure us that particle suspensions are diluted enough so that multiple-scattering effects are absent. Typical volume fractions for single scattering regime were found to lie between 10^{-7} and 10^{-6} (this corresponds to a particle density of about 10^{13}–10^{14} particles/cm^3). For the working wavelength, refractive indices have been taken as $3.101 + i0.481$ for hematite[6,7] and 1.3368 for water.[2]

4. RESULTS AND DISCUSSION

Scattered light in both full and depolarized modes was measured at angles $\theta = 20°$–$140°$ at $10°$ intervals; the normalization angle was $\theta_0 = 20°$. The experimental data $i_{exp}(\theta)$ were then fitted to

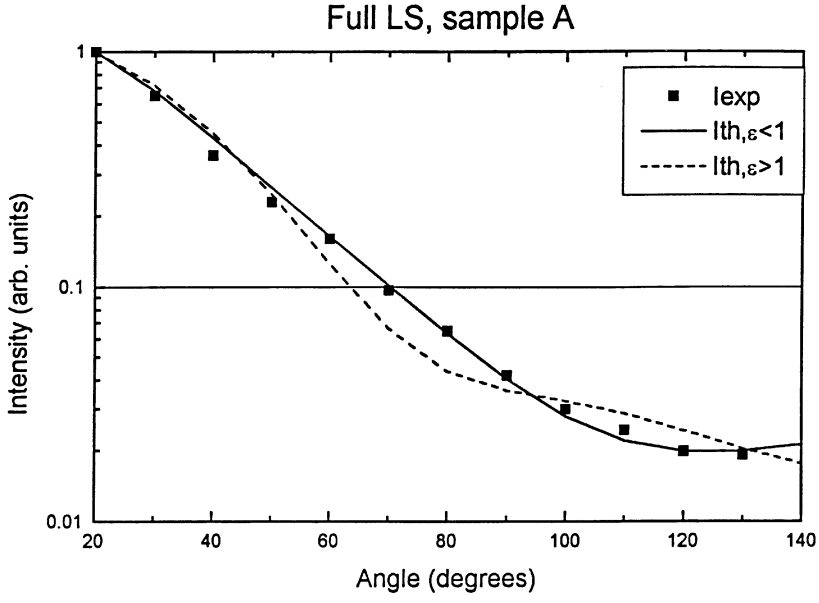

Fig. 2. Intensity vs. angle (experiment and theoretical fit) for full scattering, sample A.

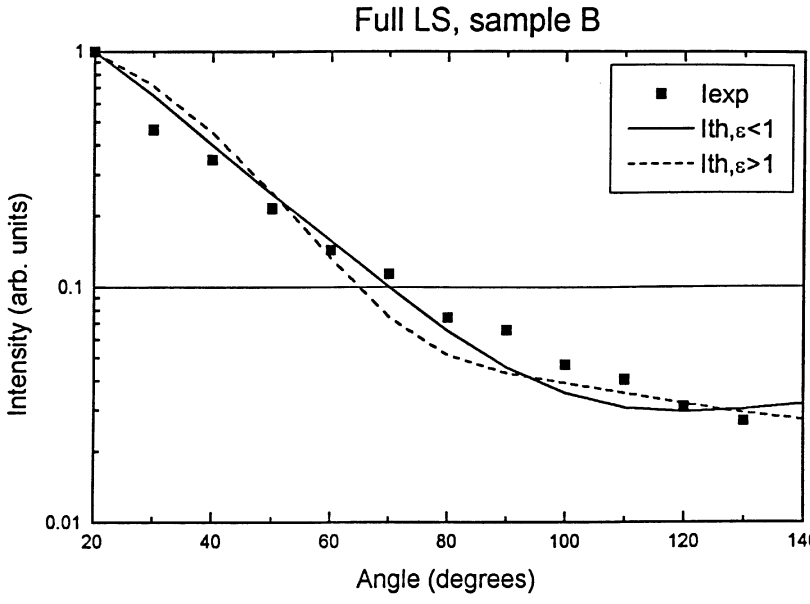

Fig. 3. Same as Fig. 2, for sample B.

Table 2. Results of computer fits on experimental data for full scattering

Sample	Method	d_{eq} (nm)	ε	ERR
A	EM	160	0.3	
	EBCM ($\varepsilon < 1$)	264	0.24	0.56900
	EBCM ($\varepsilon > 1$)	230	5.5	0.81061
B	EM	210	0.4	
	EBCM ($\varepsilon < 1$)	251	0.26	0.08625
	EBCM ($\varepsilon > 1$)	236	4.4	0.45103

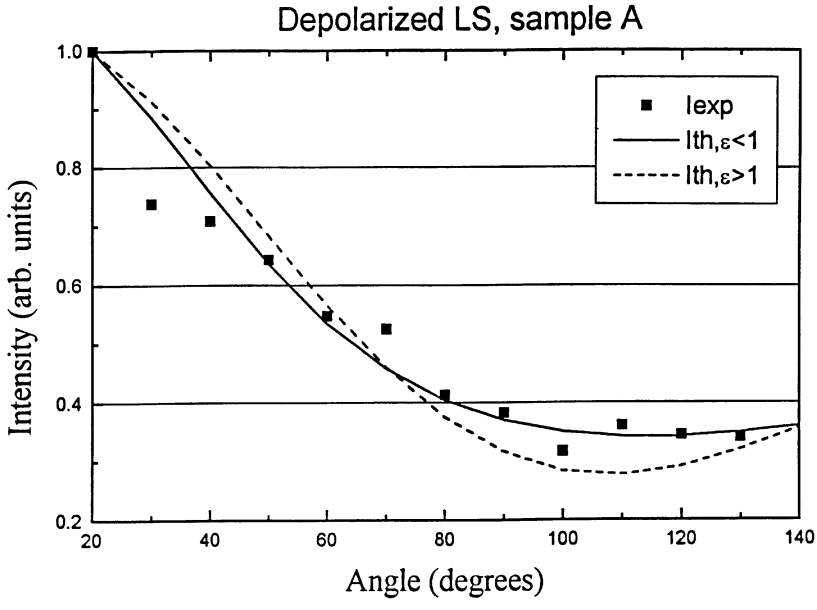

Fig. 4. Intensity vs. angle (experiment and theoretical fit) for depolarized LS, sample A.

theoretical computations of $i_{\text{th}}(\theta)$ by minimizing the total difference ERR:

$$\text{ERR} = \sum_{k=1}^{n} \left[1 - \frac{i_{\text{th}}(\theta_k, d_{\text{eq}}, \varepsilon)}{i_{\text{exp}}(\theta_k)} \right]^2 \tag{13}$$

Figures 2 and 3 show the experimental and best-fit curves for full scattering intensity on samples A and B; sizing results are summarized in Table 2. As seen, best-fit data show differences in equivalent diameter of about 20% for sample B and 65% for sample A; eccentricities also show a 20–30% difference. A second fit has also been included for which the condition $\varepsilon > 1$ has been imposed, the reason being that typically two good fits were found with roughly the same equivalent-volume diameters, but with reciprocal values of the eccentricity ε.

These differences between theory and experiment can be due to several causes. For instance, the small but nonzero polydispersity present can affect the results, since computer fits are based on monodisperse particle calculations. Other possible causes of the discrepancy could include erroneous theoretical data due to roundoff errors, inaccuracies or convergence problems. The effect of polydispersity is difficult to quantify, but computations made for spheroidal particles[37] in the range $d_{\text{eq}} \sim 100$–200 nm suggest that the introduction of a degree of polydispersity similar to the one seen in EM data tends to alter the value of the scattering and extinction cross sections in no more than about 10%. Results from our computer program have been checked by reproducing previous results from the literature;[27,38–40] general inequalities among the elements of the Mueller matrix[40,41] provide an additional validation of the computing procedure.

In any case, that could explain discrepancies in the correct value of d_{eq}, but it is not clear how polydispersity or aggregation (if any) could alter the fit quality so as to predict particles to be oblate

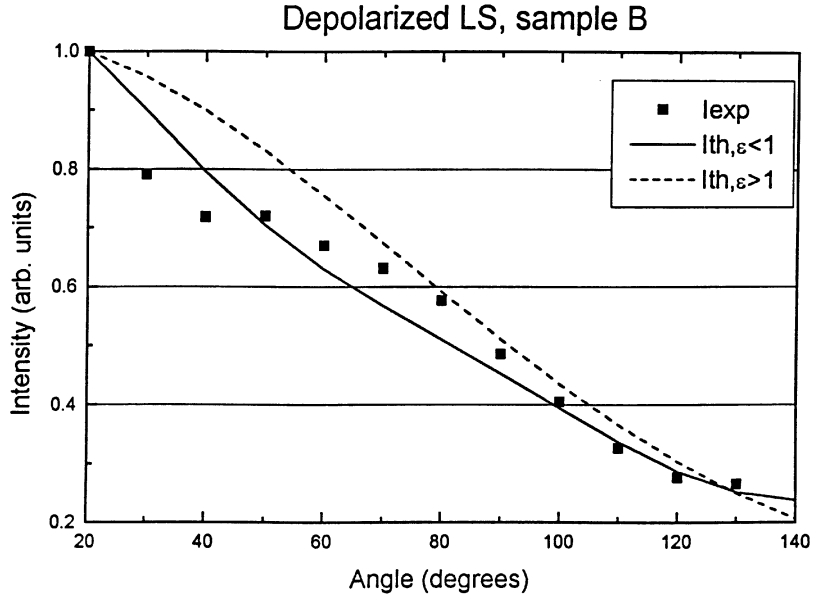

Fig. 5. Same as Fig. 4, for sample B.

Table 3. Results of computer fits on experimental data for depolarized scattering

Sample	Method	d_{eq} (nm)	ε	ERR
A	EM	160	0.3	
	EBCM ($\varepsilon < 1$)	146	0.24	0.08481
	EBCM ($\varepsilon > 1$)	113	4.6	0.22914
B	EM	210	0.4	
	EBCM ($\varepsilon < 1$)	188	0.3	0.08763
	EBCM ($\varepsilon > 1$)	96	4.0	0.25060

instead of prolate. We are then due to conclude that full scattering just does not allow to accurately size nonspherical particles in the range of interest here ($kd_{eq} \sim 1$–2 and $\varepsilon \sim 0.3$). Full scattering sizing cannot even unequivocally determine the prolateness of the samples. In order to illustrate this, two fits have been made for each sample, assuming prolate or oblate particles. It can be seen that fits for both $\varepsilon < 1$ and $\varepsilon > 1$ yield similar values of equivalent size, and roughly reciprocal values of ε. It can be seen that for both samples, $\varepsilon < 1$ fit parameter (ERR) is lower, therefore indicating a better theory-experiment agreement; however, while it is clear in sample B that fit quality is definitely better for prolate particles, it is not so for sample A, where agreement for $\varepsilon < 1$, while better than $\varepsilon > 1$, is far from satisfactory. Considering that experimental errors are always present, differences between fit parameters for oblate and prolate particles are small enough that we could not reasonably reject any

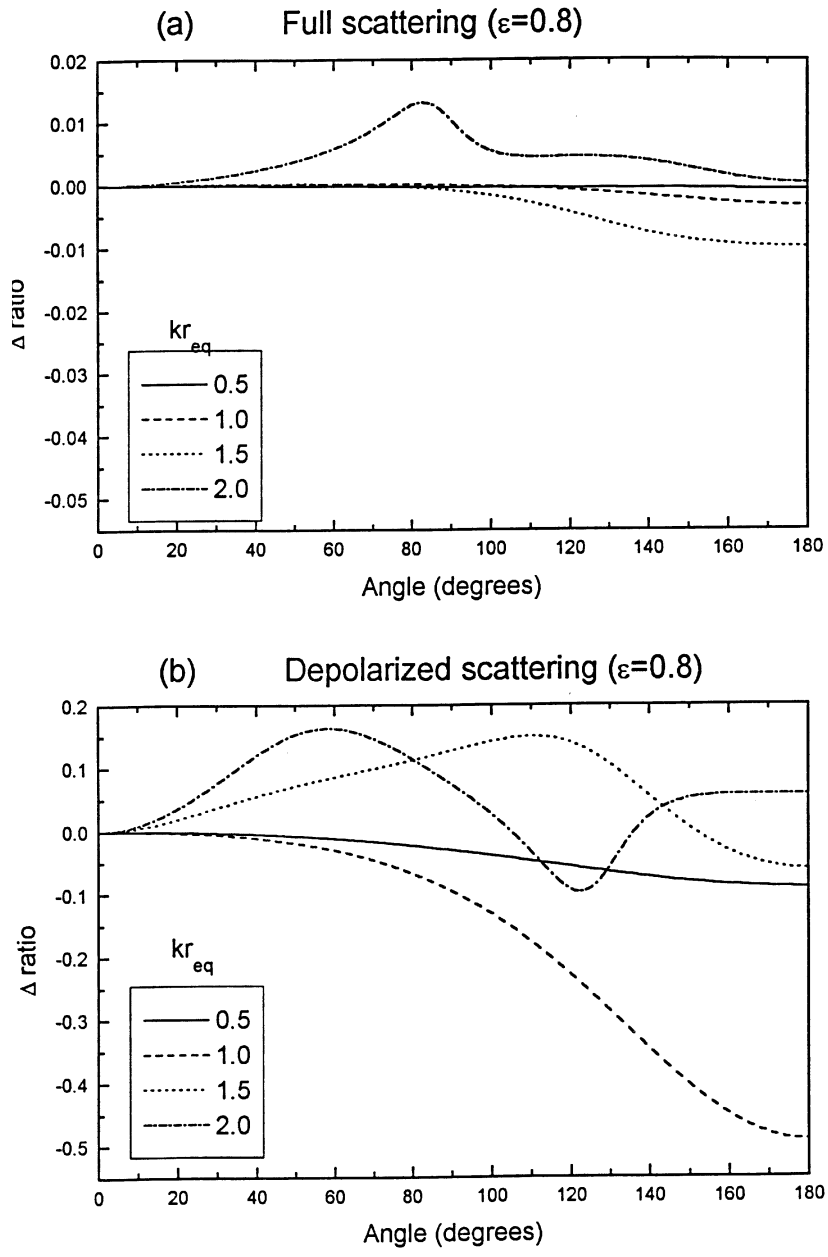

Fig. 6. Ratio $\Delta = i(\varepsilon^{-1})/i(\varepsilon) - 1$ between LS by oblate and prolate spheroids with the same volume and axial ratio $\varepsilon = 0.8$ (a) Full scattering, (b) depolarized scattering. $i(0^\circ) = 1$ in all cases. Refractive index of the particles $m = (3.101 + i0.481)/1.3368$.

of the two possibilities (in fact, LS sizing for other samples not shown here erroneously gave a best fit corresponding to *oblate* shapes[21,37]). In other words, full scattering is unable to unequivocally determine the shape character, although it yields similar values of particle volume. This axial ratio insensitivity of the element $F_{12}(\theta)/F_{11}(\theta)$ has been reported for randomly oriented spheroids, both monodisperse[42,43] and polydisperse;[44–47] cylinders in random orientation also exhibits similar curves for F_{12}/F_{11} for reciprocal values of length/diameter ratios.[47,48] Even concave and convex Chebyshev particles[49,50] show similarities in their scattering patterns for some values of the assymetry parameter e (a Chebyshev particle being obtained by rotating the curve $r(\theta) = r_0[1 + e\,\mathrm{Cos}\,n\theta]$). It gives support to the idea that aspect ratio may be a relevant parameter in linear polarization,[43,46] and indicates that sizing techniques based on this ratio could lead to serious mistakes, for the intensity and polarization patterns for prolate and oblate particles of the same size and aspect ratio are similar. If, as reported, the phase function F_{11} also shows little

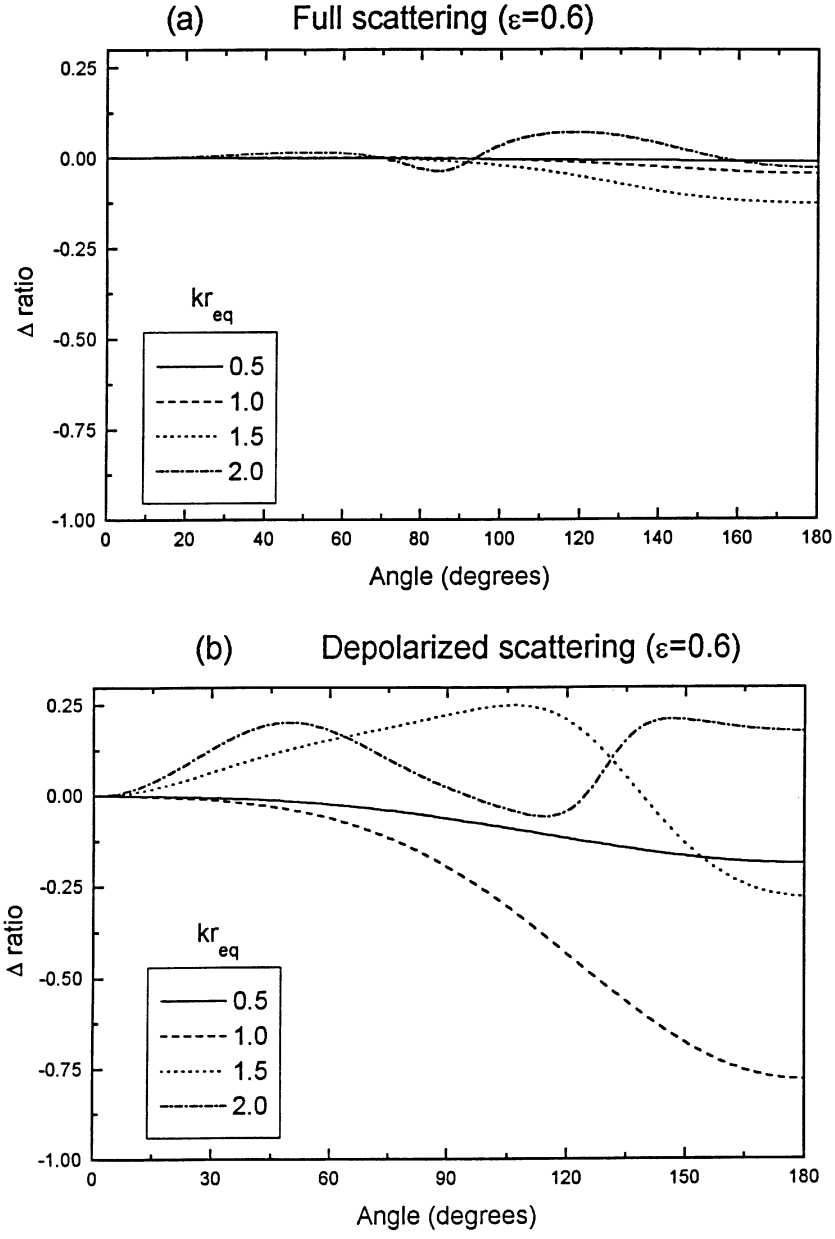

Fig. 7. Same as Fig. 6, for $\varepsilon = 0.6$.

sensitivity to the prolate/oblate character of the particles,[44,45,49–52] it could also be applicable to the difference $F_{11} - F_{12}$, as seen e.g. in Ref. 50; note that Chebyshev particles with $e = 2$ resemble, spheroids (prolate for $n = +0.1$, oblate for $n = -0.1$) and cylinders (prolate for $n = +0.2$, oblate for $n = -0.2$).

Other Mueller matrix elements can be used for particle sizing. It is generally agreed that the depolarization ratio F_{22}/F_{11} is a good measure of nonsphericity.[42,53] On the one hand, it is equal to 1 for spherical particles; therefore, any departure from unity is (in the absence of other effects such as multiple scattering or particle inhomogeneities) an indication of nonsphericity. On the other hand, it has been reported that the depolarization ratio is size and aspect ratio dependent,[40,44–46,53] so that it can be used to distinguish between prolate and oblate particles with the same size and long-to-short axes ratio. Furthermore, F_{22}/F_{11} is much more size and aspect ratio dependente for prolate spheroids than for oblate spheroids,[45] so it is expected that computer fits of the ratio F_{22}/F_{11}

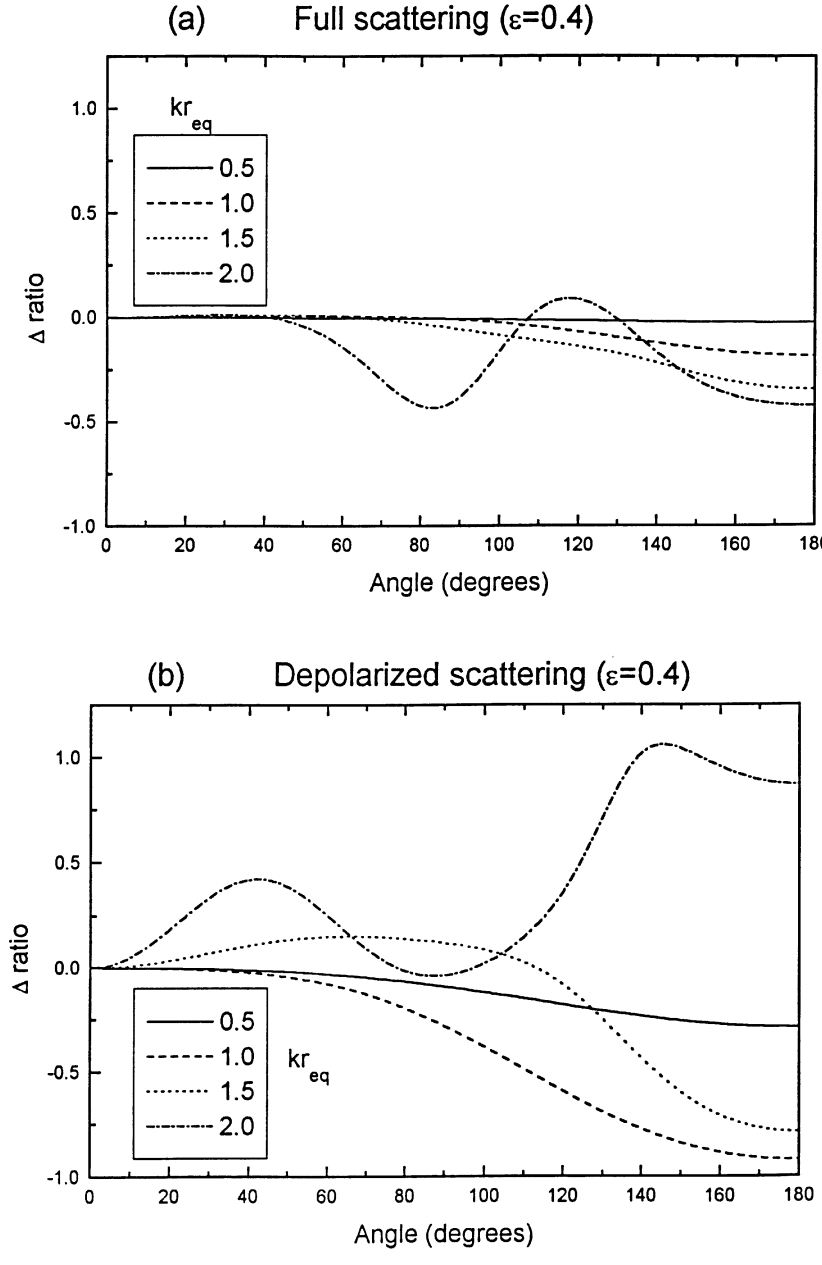

Fig. 8. Same as Fig. 6, for $\varepsilon = 0.4$.

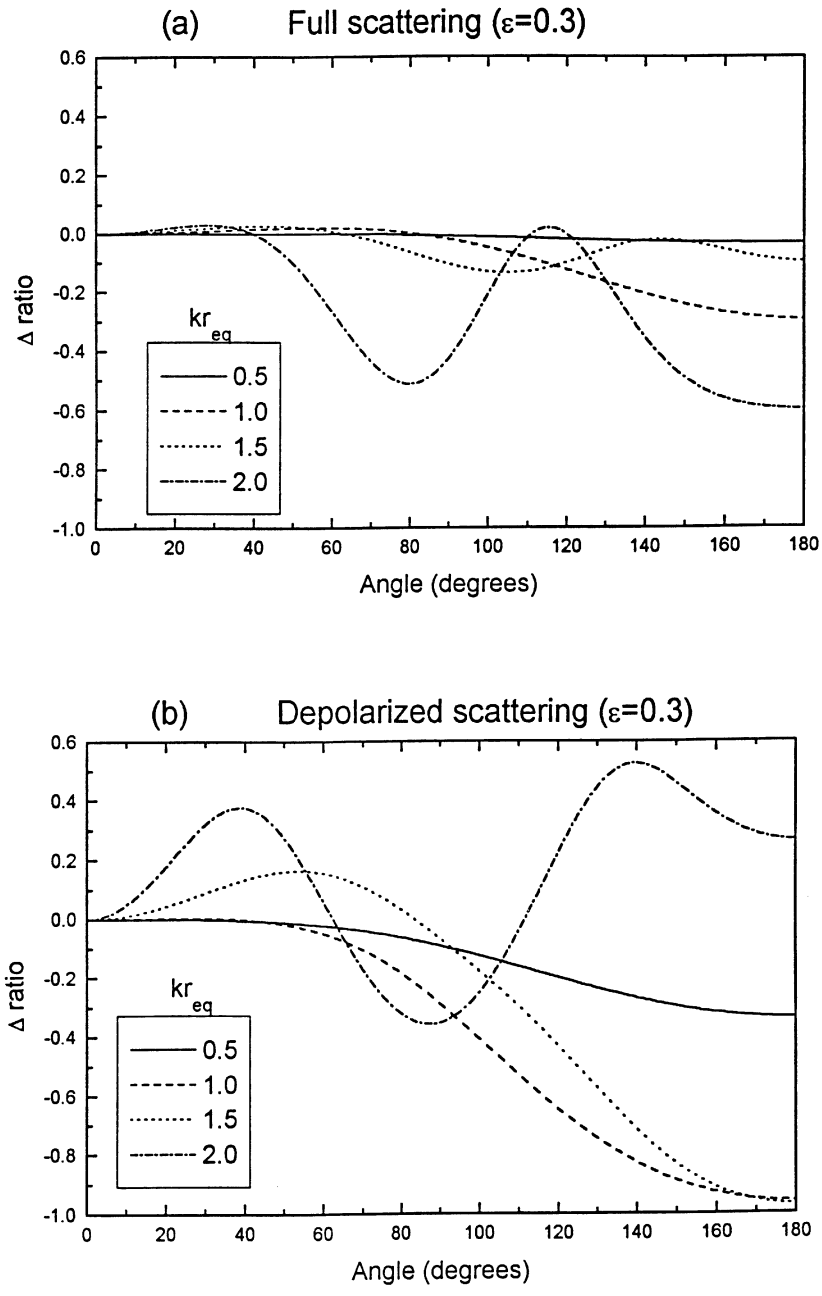

Fig. 9. Same as Fig. 6, for $\varepsilon = 0.3$.

on prolate particles give good quality results, in the sense that small differences in the measured values of intensity (due to experimental errors, for instance) do not result in large differences of the obtained values of d_{eq} and ε; the same can be said about slight differences in the calculation process due to the degree of accuracy requested.[21,39,45,50] There is also a practical reason to choose the element F_{22} as a particle sizer: it can be easily measured in the form $F_{11}(\theta) - F_{22}(\theta)$ by insertion of a polarizer between the sample and the PMT (see the Experimental Details section).

The results of the depolarized LS results can be seen in Figs. 4 and 5. Again, two best fits have been included for both $\varepsilon < 1$ and $\varepsilon > 1$. Results are shown in Table 3. As it can be seen, both samples are correctly identified as made up of prolate particles, and the values of d_{eq} so obtained compare better to the EM data, coinciding to within 10%; the predicted value of d_{eq} for the oblate fit is even worse than it was in the case or full scattering. Even though the depolarized signal was found to be 2–3

orders of magnitude weaker than the full signal, the agreement between observation and computation lead us to think of depolarized LS as a valuable tool for sizing of nonspherical particles, including correct determination of its prolate-oblate nature.

In order to show the qualities of depolarized LS as compared to full LS for determination of the axial ratio nature, a set of calculations have been performed for the same refractive indices (3.101 + i0.481 for the particle, 1.3368 for the medium) and equivalent-size dimensionless parameter kr_{eq} in the range 0.5–2. Figures 6–9 show the ratio $\Delta = i(\varepsilon^{-1})/i(\varepsilon) - 1$ for values $\varepsilon = 0.3$, 0.4, 0.6 and 0.8, where $i \sim F_{11} - F_{12}$ for full scattering and $i \sim F_{11} - F_{22}$ for depolarized scattering; in all cases the convention $i(\theta = 0^\circ) = 1$ was adopted, which forces $\Delta(0^\circ) = 0$ in all cases. It can be seen that all curves show nonzero values of Δ at angles near $\theta = 180^\circ$, which corresponds to the well-known size/shape sensitivity of scattering in the backward direction.[15,43] In can be seen in these figures that the differences between equal-volume oblate and prolate particles are much larger for the case of depolarized scattering than for full LS, as it was found out during the fit procedure. It cannot be said that full LS curves are equal for all oblate/prolate pairs, regardless of their size and eccentricities; $\varepsilon = 0.4$ and 0.3 are good counterexamples. Neither we try to hold these results as representative for any size/shape/refractive index combination. But, in view of our experimental results and computer predictions, we can conclude that, within the size range $kr_{eq} \sim 0.5$–2, depolarized LS ($F_{11} - F_{22}$) is a valuable sizing tool for natural systems under non-perfect conditions (e.g. moderately low polydispersity), while full LS ($F_{11} - F_{12}$) can provide a first approximation of the equivalent size of the particle. We also acknowledge the limitation of this predictions, since they have been experimentally tested on highly absorbing particles, but the agreement with similar predictions for less absorbing particles leads us to think that it might be a common feature for all kinds of particle materials, thus constituting a valuable LS fingerprint for the determination of size and axial ratio up to a certain particle size.

Acknowledgements—Financial support for this research was provided by DGICYT, Spain (Proj. # PB94-0812-C02-1).

REFERENCES

1. Mie, G., *Ann. Phys*., 1908, **25,** 377.
2. Kerker, M., *The Scattering of Light and Other Electromagnetic Radiation*. Academic Press, San Diego, 1969.
3. Bohren, C. F. and Huffman, D. R., *Absorption and Scattering of Light by Small Particles*. Wiley, New York, 1983.
4. Pinnick, R. G., Rosen, J. M. and Hofmann, D. J., *Appl. Opt*., 1973, **12,** 37.
5. Ray, A. K., Souyri, A., Davis, E. J. and Allen, T. M., *Appl. Opt*., 1991, **30,** 3974.
6. Hsu, W. P. and Matijević, E., *Appl. Opt*., 1985, **24,** 1623.
7. Kerker, M., Scheiner, P., Cooke, D. D. and Kratohvil, J. P., *J. Colloid Interface Sci*., 1979, **71,** 1761.
8. Heller, W. and Wallach, M. L., *J. Phys. Chem*., 1964, **68,** 931.
9. Kerker, M., Matijević, E., Espenscheid, W. F., Farose, W. A. and Kitani, S., *J. Colloid Interface Sci*., 1964, **19,** 213.
10. Gledhill, R. J., *J. Phys. Chem*., 1962, **66,** 458.
11. Melik, D. H. and Fogler, H. S., *J. Colloid Interface Sci*., 1983, **92,** 161.
12. Walstra, P., *J. Colloid Interface Sci*., 1968, **27,** 493.
13. Zollars, R. L., *J. Colloid Interface Sci*., 1980, **74,** 163.
14. Mulholland, G. W., Hartman, A. W., Hembree, G. G., Marx, E. and Lettier, T. R., *J. Res. Natl. Bur. Stand*., 1985, **90,** 3.
15. Bohren, C. F. and Singham, S. B., *J. Geophys. Res*., 1991, **96,** 5269.
16. Waterman, P. C., *Phys. Rev. D*, 1971, **3,** 825.
17. Barber, P. W., *IEEE MTT*, 1977, **25,** 373.
18. Scheiner, J. B. and Peden, I. C., *IEEE AP*, 1988 **36,** 1317.
19. Stratton, J. A., *Electromagnetic Theory*. McGraw-Hill, New York, 1991.
20. Tsang, L., Kong, J. A. and Shin, R. T., *Radio Sci*., 1984, **19,** 629.
21. Quirantes, A., Ph.D. Thesis, Universidad de Granada, 1994.
22. Stein, S., *Quart. J. Appl. Math*., 1961, **19,** 15.
23. Cruzan, O. R., *Quart. J. Appl. Math*., 1962, **20,** 33.
24. Mishchenko, M. I., *Astrophys. J*., 1990, **367,** 561.
25. Siewert, C. E., *Astrophys. J*., 1981, **245,** 1080.
26. Hovenier, J. W. and van der Mee, C. V. M., *Astron. Astrophys. J*., 1983, **128,** 1.
27. Mishchenko, M. I., *J. Opt. Soc. Am. A*, 1991, **8,** 871; errata, *ibid*. 1992. **9,** 497.
28. Meehan, E. J. and Beattie, W. H., *J. Phys. Chem*., 1960, **64,** 1006.
29. Wyatt, P. J., *J. Colloid Interface Sci*., 1972, **39,** 479.

30. Quirantes, A., Plaza, R. and Delgado, A., *J. Colloid Interface Sci.*, 1997, **189,** 236.
31. Reagan, J. A., Byrne, D. M., King, M. D., Spinhirne, J. D. and Herman, B. M., *J. Geophys. Res.*, 1980, **85,** 1591.
32. Seliga, T. A. and Bringi, V. N., *J. Appl. Meteorol.*, 1976, **15,** 69.
33. Matijević, E. and Scheiner, P., *J. Colloid Interface Sci.*, 1978, **63,** 509.
34. Ozaki, M., Kratohvil, S. and Matijevic̀, E., *J. Colloid Interface Sci.*, 1984, **102,** 146.
35. Morales, M. P., González-Carraño, T. and Serna, C. J., *J. Mater. Res.*, 1992, **7,** 2583.
36. Sugimoto, T., Muramatsu, A., Sakata, K. and Shindo, D., *J. Colloid Interface Sci.*, 1993, **158,** 420.
37. Quirantes, A. and Delgado, A. V., *Appl. Opt.*, 1995, **34,** 6256.
38. Heller, W. and Pangonis, W. J., *J. Chem. Phys.*, 1957, **26,** 498.
39. Barber, P. W. and Hill, S. C., *Light Scattering by Small Particles*: *Computational Methods*. World Scientific, Singapore, 1990.
40. Kuik, F., Ph.D. Thesis, Free University, Amsterdam, 1992.
41. Fry, E. S. and Kattawar, G. W., *Appl. Opt.*, 1981, **20,** 2811.
42. Asano, S. and Sato, M., *Appl. Opt.*, 1980, **19,** 962.
43. Schuerman, D. W., Wang, R. T., Gustafson, B. Å. and Schaefer, R. W., *Appl. Opt.*, 1981, **20,** 4039.
44. Mishchenko, M. I. and Travis, L. D., Atmospheric propagation and remote sensing II, *SPIE*, 1993, **1968,** 118.
45. Mishchenko, M. I., *Appl. Opt.*, 1993, **32,** 4652.
46. Mishchenko, M. I. and Travis, L. D., *Appl. Opt.*, 1995, **33,** 7206.
47. Mishchenko, M. I. and Travis, L. D., *JQSRT*, 1994, **51,** 759.
48. Mishchenko, M. I., *Appl. Opt.*, 1996, **35,** 4927.
49. Wiscombe, W. J. and Mugnai, A., *Appl. Opt.*, 1988, **27,** 2405.
50. Wiscombe, W. J. and Mugnai, A., *NASA Ref. Publ.*, 1157, NASA/GSFC. Greenbelt, MD, 1986.
51. Hill, S. C., Hill, A. C. and Barber, P. W., *Appl. Opt.*, 1984, **23,** 1025.
52. Mishchenko, M. I., Travis, L. D., Kahn, R. A. and West, R. A., *J. Geophys. Res.*, 1997, **102,** 16831.
53. Perry, R. J., Hunt, A. J. and Huffman, D. R., *Appl. Opt.*, 1978, **17,** 2701.